Bubble Entrapment and Stability in Complex Passageways

John Geile; Yongkang Chen; Mark M. Weislogel; Portland State University, Portland, OR/USA; Trevor Snyder; Global Development Group, Xerox Corporation, Wilsonville OR/USA

Abstract

The presence of bubbles in the complex passageways of inkjet print heads can cause a variety of ill-effects from changes in local wave dampening to droplet misfire and ejection asymmetry leading to weak, intermittent, chronically missing jets or defects leading to crosstalk. In this study we present macroscale observations of capillarity-driven flow phenomena in simulated rectangular microchannels. The high resolution video results are gathered following brief experiments conducted in a drop tower which enables the use of large length scale transparent channels with representative flows that are readily captured at 60 fps. Conduit geometries simulating unit tortuous passageways in print head stacks are studied identifying geometries that inadvertently generate bubbles during in-fill or re-fill. The flow in each channel is interrupted by a 'feature,' the geometry of which is systematically varied to identify critical shapes and flow rates. The mechanisms for such bubble generation and entrapment depend strongly on the feature geometry, where if local capillary flow rates exceed global flow rates the bubble entrapment does not occur. Scaling laws and numerical computations are employed to predict the critical flow rate conditions under which such entrapment may be avoided.

Introduction

Inkjet systems are growing both in scale and in breadth of applications and include both traditional printing and new industrial and 3D applications. To satisfy the requirements for throughput, quality, materials compatibility, and reliability, printhead manufacturers are continuing to improve their designs and are driving for more nozzles per inch, smaller drops, and other value-added features. However, development costs for a printhead are high. Therefore in any new design, it is important to build a foundation with performance, flexibility and robustness in mind. For example, to achieve a multi-color printhead with similar performance, cost, and jet density as compared to a single color printhead leads to substantially more complexity in the fluid path. Designs such as this require better measurement methods and numerous innovations. A detailed view of such a design is shown in Fig. 1. The structure is composed of many complex fluidic features including: 1) 'Finger' manifolds; 2) body-side view of two colors interleaved; 3) two other colors interleaved; 4) aperture-side view of two colors interleaved; 5) two other colors interleaved; 6) "Main" manifolds [1]. The drop mass, number of jets, and jetting frequency together determine the flow rate of the printhead and the inherent resolution. Smaller drops are better for some applications (photo-quality images), while larger drops can be optimal for many industrial applications (ceramics, masking, textiles, 3D printing, and other industrial applications). Multiple color head designs allow for greater flexibility, however, other performance characteristics cannot be sacrificed.

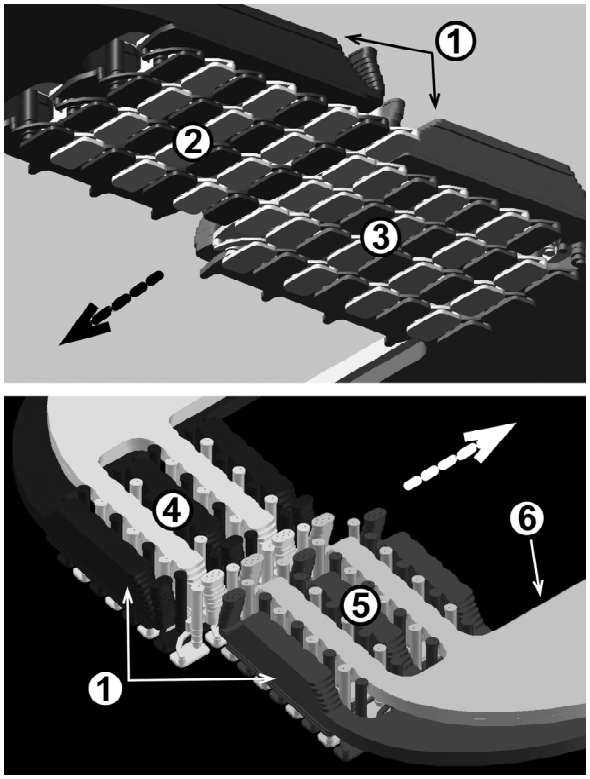

***Figure 1**. Multi-color print head fluid path design.*

Certain flow phenomena within ink jet print heads are difficult to fully quantify due the intricate, microscopic, and opaque passageways that carry the capillary liquids driven at high frequencies; typically on the order of 10 kHz corresponding to the natural frequencies of the capillary surfaces in the nozzles ~ $(\sigma/\rho R^3)^{1/2}$; where σ, ρ, and R are the liquid surface tension, density, and nozzle radius, respectively. Nozzle radii R on the order of 10 μm are common.

It is noteworthy that similar capillary fluidic phenomena arise in the nearly weightless state found aboard many spacecraft, but over dramatically increased length scales. For example, it is thoroughly intriguing to imagine an ink jet of nozzle radius of one meter! But such is possible in a 'micro-gravity' environment and leads to fundamental natural frequencies as low as ~ 0.005 Hz—a 10^6-fold reduction compared to the terrestrial equivalent. As a result, experiments relating to inkjet capillary fluidics can be slowed by many orders of magnitude by performing them in reduced gravity environments employing larger sized systems. The flow phenomena may be filmed at normal video frame rates

without magnification and the test cells may be constructed of transparent materials using established methods allowing complete optical access.

In this study a variety of rectangular channels of millimetric cross section are placed in a drop tower where they experience spontaneous capillary rise following the step reduction in gravity associated with entry into free fall. The channel sections chosen are related to print head stack channel geometries and include abrupt features that are often found in such conduits. Though any number of investigations might be pursued [2], our focus here is on the inadvertent formation of bubbles in such channels during capillary-driven flow and what becomes of such bubbles once the flow has past. This work is synergetic with numerous different applications, however, the current focus is on fluids path design for inkjet print heads with other applications inferred.

Description of Experimental Approach

A typical drop tower capillary rise experiment is shown schematically in Fig. 1. An experimental platform called a rig is employed which contains the experiment, backlight, and 60fps HD camera. For each experiment, while the rig is hanging within the drag shield of the drop tower [2], a test cell is placed in a support which connects the channel base with a brimming fluid reservoir. The experiment, test rig, and drag shield are then simultaneously released for 2.1s of free-fall. Each drop experiment is performed three times; once initially dry and twice after being wetted by the fluid. Typical results are shown in Fig. 2.

When the capillary channel is complex [3] one finds that such features can create bubbles that are either entrapped or released into the flow. When the capillary flow velocities are high enough, Fig. 3 demonstrates how bubbles are generated during the spontaneous capillary flows in channels and the different outcomes of entrapment and expulsion. Characteristic dimensions are identified in Fig. 3a. These drop tower experiments examine rectangular channels with blind 'features'. Once the fluid reaches a feature, capillary forces quickly wick fluid into it along its interior edges. If the time required for the bulk flow to pass the feature is less than the time required to fill the feature due to the feature corner wetting phenomenon, the fluid will bypass the gas contained within the feature and continue along the main channel; essentially generating a bubble within the feature. Such bubbles may remain entrapped or be displaced and drawn into the main channel flow. The outcome is dependent on the feature geometry, bulk velocity, and fluid properties.

A variety of the test cell conduit feature types investigated are depicted in Fig. 4. The acrylic cells are constructed from 2-D CAD models that are printed using a laser cutter in 3 mm thick transparent acrylic sheets as depicted in the exploded view of Fig. 5. The cells typically consist of three layers sealed together by double-sided adhesive tape placed on both sides of the central layer prior to cutting. The non-adhesive backing is then removed from the tape, the layers are aligned, and the assembly is pressed together in a vice to form a tight seal.

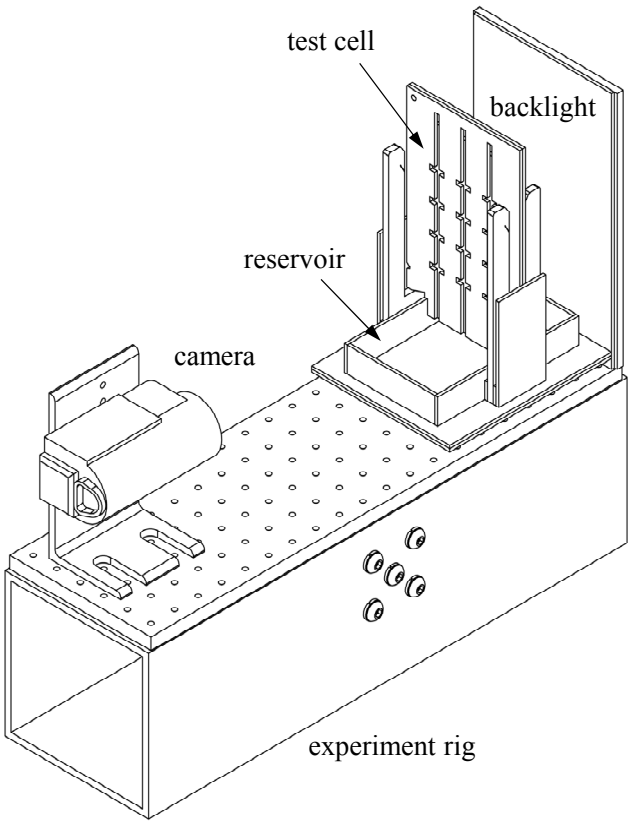

***Figure 1**. Solid model of an experiment rig with HD camera, backlight, integral test cell holder and reservoir, and test cell.*

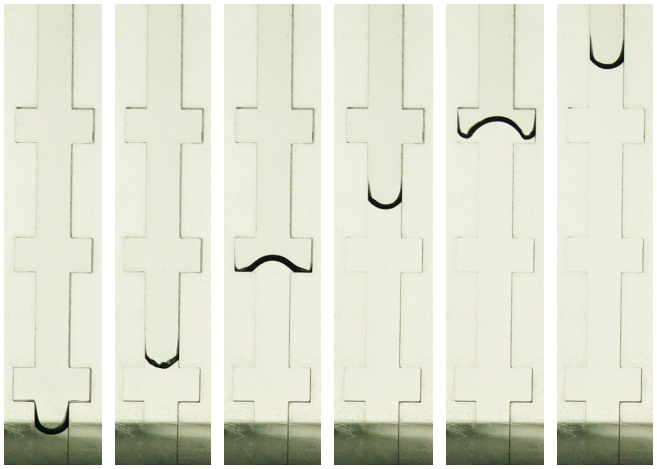

***Figure 2**. 6 Hz images of a drop tower test of sudden capillary rise of perfectly wetting 0.65 cs PDMS in a single rectangular channel with serial blind features. The meniscus advances passively without generating bubbles within the features.*

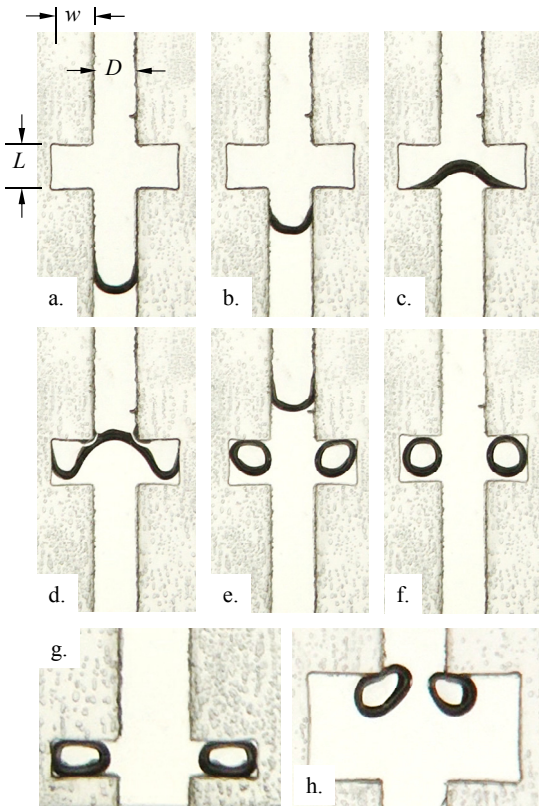

***Figure 3**. a.-f. A sequence of images of spontaneous capillary rise in a drop tower using a D = L = w = 5 mm rectangular channel of thickness δ = 3mm leading to bubble generation and entrapment within a blind feature. Three primary categories of bubble generation within channels are identified herein: f. unconfined entrapment, g. confined entrapment, and h. generation with expulsion. Images g. and h. are taken from separate drop tests.*

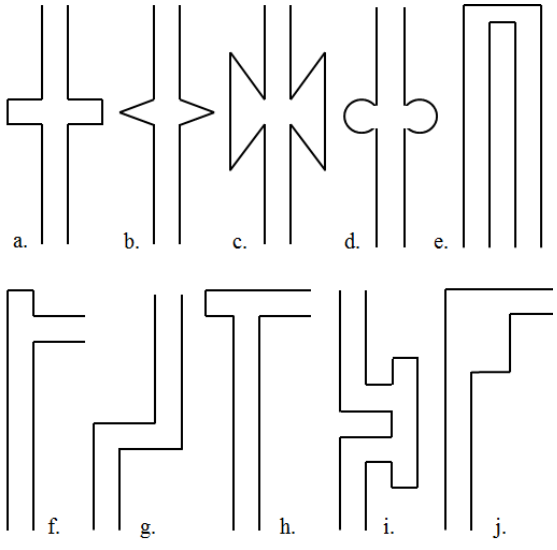

***Figure 4**. Channel feature shapes tested for bubble generation/entrapment. Dimensions are varied for each feature type.*

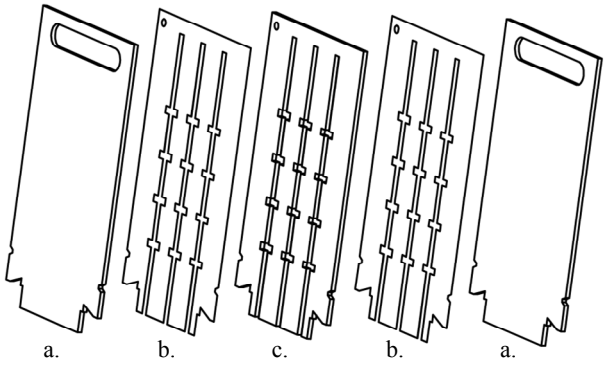

***Figure 5**. Assembly view of characteristic test cell (Ref. Figs. 1 and 2): a. front and back acrylic channel covers with gas exit ports, b. double-sided tape with channel cut-outs, and c. acrylic channel. This test cell employs three parallel channels.*

Experimental Results

The video results are converted into still image files for subsequent data reduction. The bubble generation phenomenon may be mapped noting the channel geometry and meniscus velocities collected from such images. For example, a sample regime map for 0.65 PDMS is presented in Fig. 6 of entrapment as a function of bulk meniscus velocity V_D and channel feature geometry function $\phi \equiv \delta H/L^2$ (xx consistent notation), where δ is the channel depth, L is the feature length, and H is the shorter of either the length L of feature thickness δ. The map identifies regions of bubble generation with entrapment or expulsion as well as cases where no generation occurs. The figure includes the results of 80 drop tests, employing 240 test channels, with 711 features. (Note: The bottleneck in the experimental procedure is the image processing. In support of this research a total of 180 drop tests have been conducted to date with a maximum of 55 completed in one 8 hour working day.) Such maps will differ from mechanically pumped flows due to the fact that these flows are driven by meniscus curvature which is highly distorted by the abrupt feature geometry. Scenarios other than simple generation, entrapment, and expulsion include generation with partial expulsion where the remaining entrapped bubble is either confined or unconfined within the feature.

For a bubble to be generated within the feature, the time t_c required for the capillary fluid to cross the feature length L must be less than the amount of time t_f needed for the capillary fluid to wick into and fill the feature. To ensure that the bubbles entrap, $t_c/t_f \ll 1$. The time to cross the feature scales as $t_c \sim L/V_D$. Invoking demonstrated scales for the corner wicking flow within each feature it can be shown that [4]

$$t_f \sim K\mu w^2/(0.086\sigma H), \qquad (1)$$

where μ is the dynamic viscosity of the test fluid and K is a factor used to qualitatively estimate the total time to fill a feature. The coefficient 0.086 is calculated from known quantities for wicking along 90º interior corners with a perfectly wetting fluid. Therefore, employing eq. (1), entrapment is highly likely to occur when

$$t_c/t_f \sim 0.086\phi\sigma/(K\mu V_D) \equiv 0.086\phi/K\mathrm{Ca} \ll 1, \qquad (2)$$

where $K \geq 100$ is typical and $\text{Ca} \equiv \mu V_D/\sigma$, where Ca is the local capillary number for the flow.

As illustrated in Fig. 6, the relationship between the feature geometry ratio ϕ and the incoming velocity V_D of the fluid is clear from the figure—the likelihood of bubble generation increases with meniscus velocity. In fact, the dividing line between no bubble generation and bubble generation appears to be linear for the majority of points collected and an approximation is provided by the dashed line and equation in Fig. 6. Within the bubble generation region, as ϕ increases the entrapped bubbles transition from the entrapped confined, entrapped unconfined, and the fully expelled varieties (ref. to Figs. 2g, 2f, and 2h, respectively).

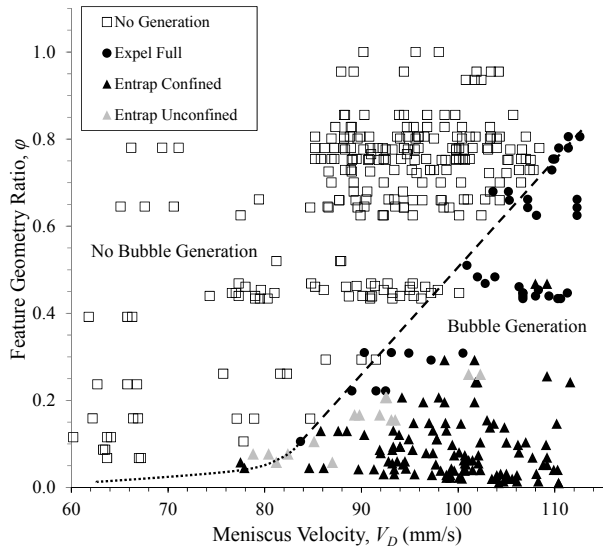

***Figure 6**. Regime map of dimensionless feature geometry parameter ϕ vs. meniscus velocity V_D for the channel type of Fig. 4a. The legend identifies the observed bubble behavior after the bulk meniscus in the main channel passes the feature. An approximately linear zone divides the bubble generation-no generation regimes as identified by the dashed line approximated by $\phi = 0.0236V_D - 1.84$. The dotted line is the expected trend for $\phi \rightarrow 0$.*

The results of such experiments can be used as a guide for setting tolerance levels for features within the passageways of solid ink and inkjet print heads. They can also be used quantitatively to determine ideal feature geometries to liberate entrapped gases created during start-up, system cycling, or during off-nominal operations. An example is provided in Fig. 7, where the otherwise rectangular channel possesses asymmetric triangular or wedge-shaped features. Bubble generation in such features leads to certain expulsion due to two mechanisms. The first is the already described local capillary corner wicking phenomena. But in this case the capillary forces continue to draw the liquid fully into the feature displacing the bubble into the main flow channel. During this process the bubble begins to partially occlude the main passageway causing local accelerations in the liquid around the bubble to maintain the liquid flow rate i.e., a Bernoulli effect. The accelerating fluid reduces local pressures that also aid to draw the bubble into the bulk flow. Such geometries passively generate bubbles which are then passively liberated and swept further downstream where they may continue to interact (i.e. merge, as shown in Fig. 7) with the flow. Note that the expulsion example shown in Fig. 2h is the result of the combined capillary displacement and Bernoulli effects.

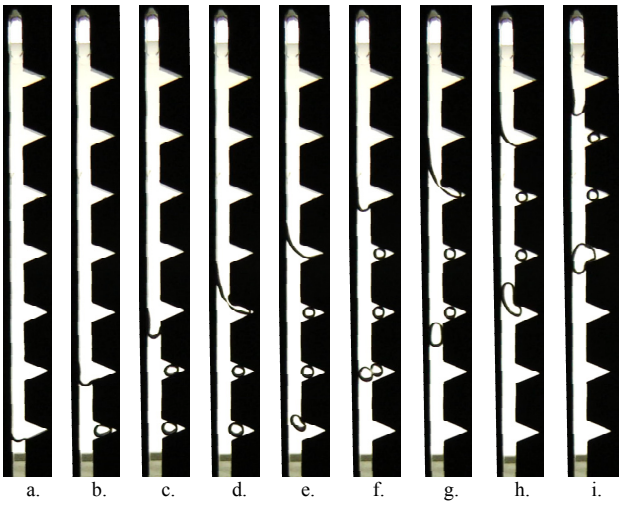

***Figure 7**. Drop tower test of passive bubble generation and expulsion in a rectangular channel with asymmetric wedge-shaped features. The 6Hz images show b. bubble generation followed by e. expulsion where the f. liberated bubbles merge with entrapped bubbles downstream collecting all generated bubbles into i. one large gas slug which eventually catches up with the bulk meniscus sweeping the flow clear of bubbles before the process repeats.*

Numerical Approach

Once bubbles are entrapped their mobility becomes dependent on the stability of the new bubble-channel system and the orientation of gravity with respect to the channel axis. For a quiescent fluid, the static stability criterion is determined by a balance of gravitational and surface tension forces. Because of the latter's strong dependence on wetting conditions, feature geometry, and bubble volume, even slightly un/favorable gravity vectors are capable of destabilizing and thus liberating the entrapped bubbles.

For example, critical bubble volumes as a function of complex channel geometry may be determined feeding back design guides that encourage self-purging mechanisms in the head stack. A prebuilt numerical model of a highly variable channel geometry is provided for general design purposes using the recently open-sourced SE-FIT software [5]. SE-FIT runs K. Brakke's Surface Evolver algorithm [6] to compute minimal surface energy configurations. The user-friendly design tool is highly configurable and provides the designer with both an educational and practical look into the wide variety of capillary outcomes arising from a strong dependence on complex geometry.

A sample computational domain is provided in Fig. 8 for a perfectly wetting liquid. It is clear that entrapped bubbles of this type are unstable with respect to the gravity vector depending on the bubble volume. Stable configurations are shown in Fig. 9 for increasing bubble volumes with the critical bubble volume condition shown in Fig. 9d for this particular selection of feature dimensions, g-magnitude, and in-plane g-orientation angle ϕ. The SE-FIT pre-built model is highly variable and may be used to determine self-purging geometries if control of conduit orientation

is provided. Plots such as that shown in Fig. 10 for the geometry of Fig. 8 may be constructed providing critical bubble volumes that are useful in design.

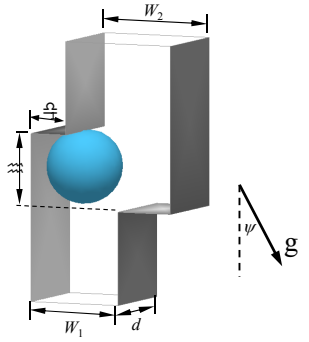

***Figure 8**. Schematic of an entrapped bubble in a rectangular channel feature. The notation identified is used to characterize the geometry of the problem for numerical calculations of bubble stability limits as a function of g and g-orientation angle ϕ = 35º.*

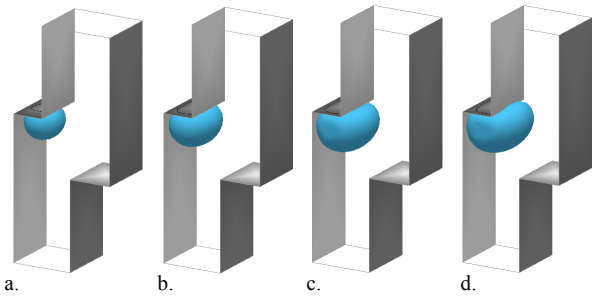

***Figure 9**. Stable computed surfaces as a function of bubble volume for Bo=2 and ϕ = 35º (w_1 = 2,d = 2,w_2 = 2.4, η = 1.8). The surface of d is the last stable interface beyond which the bubble detaches and leaves the channel junction.*

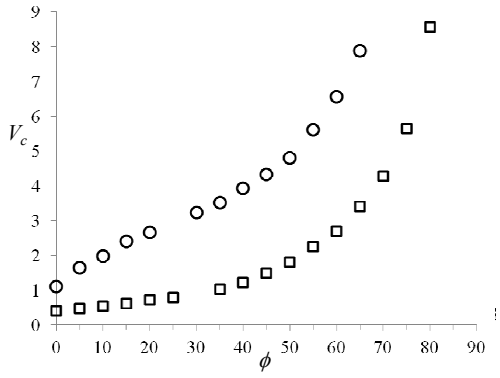

***Figure 10**. Numerical results of critical volume vs. g-orientation angle ϕ at different δ_1 and Bo = 2.Circles are for δ_1 = 1 and squares are for δ_1 = 0.5. The half of the upstream channel width is the characteristic length. Such data is readily computed using the Parameter Sweep Function within the SE-FIT software [4].*

Discussion and Directions

This work provides an example of how capillary fluidic phenomena relevant to inkjet printing can be pursued employing drop towers. Large capillary systems may be studied systematically using affordable low speed HD video photography and test cells constructed of transparent materials using routine methods. Other methods to study droplet ejection, dynamics, impacts, etc. [2] can also benefit from experimentation in a drop tower. Relating to flows within print head stacks, for the case of bubble generation, entrapment, and expulsion from abrupt features along capillary conduits, experimental results provided herein show how the local geometry promotes or retards such behavior. Control of specific geometry may be exploited to assure a desired outcome, or protect against an undesired one. This work addresses purely capillary driven flows, but it is straightforward to conduct such investigations using mechanically pumped flows that are more akin inkjet printing.

References

[1] S. Korol, "An Analysis of Recent Advances in Solid Ink Printer Performance from a Print Head Perspective", Proc. NIP24, pg. 107 (2008).

[2] Wollman, A., Weislogel, M., New Investigations in capillary fluidics using a drop tower, Experiments in Fluids, Vol. 54, Issue 4, p 1499, April 2013.

[3] Lenormand, R., Zarcone, C., Sarr, A. (1983) Mechanisms of displacement of one fluid by another in a network of capillary ducts, *J. Fluid Mech*., Vol 135, pp 337-353.

[4] M.M. Weislogel, Baker, J.A., Jenson, R.M., Quasi-steady capillarity-driven flows in slender containers with interior edges, J. Fluid Mech., Vol. 685, 271-305 (2011).

[5] Y. Chen, B.M. Schaeffer, M.M. Weislogel, G.A. Zimmerli, Introducing SEFIT: A Surface Evolver Based Tool for Studying Capillary Surfaces, AIAA-2011-1319, 11 pages, 49th AIAA Aerospace Sciences Meeting, 4-7 January 2011, the software is available at http://se-fit.com/.

[6] K.A. Brakke, The Surface Evolver, Experimental Mathematics, Vol. 1, No. 2, 1992, pp. 141, 165, the code and manual are available at http://www.susqu.edu/facstaff/b/brakke/.

Author Biography

John Geile is a recent BSME graduate from Portland State University (PSU) where he became involved with studies of capillary fluidics in microgravity using a drop tower. Y. Chen and M.M. Weislogel are faculty at PSU with significant experience in large length scale capillary flow experiments and analysis. Dr. T. Snyder is a Principal Scientist working for Xerox in Wilsonville Oregon. This work was funded by a Xerox University Affairs Grant.